Intense 1.5-cycle near infrared laser waveforms and their use for the generation of ultra-broadband soft-x-ray harmonic continua

New Journal of Physics
The open-access journal for physics

Intense 1.5-cycle near infrared laser waveforms and their use for the generation of ultra-broadband soft-x-ray harmonic continua

A L Cavalieri[1,3], E Goulielmakis[1], B Horvath[1], W Helml[1], M Schultze[1], M Fieß[1], V Pervak[2], L Veisz[1], V S Yakovlev[2], M Uiberacker[2], A Apolonski[2], F Krausz[1] and R Kienberger[1,3]

[1] Max-Planck-Institut für Quantenoptik, Hans-Kopfermann-Str. 1, D-85748 Garching, Germany

[2] Department für Physik, Ludwig Maximilians Universität, Am Coulombwall 1, D-85748 Garching, Germany

E-mail: adrian.cavalieri@mpq.mpg.de or reinhard.kienberger@mpq.mpg.de

New Journal of Physics **9** (2007) 242
Received 20 June 2007
Published 31 July 2007
Online at http://www.njp.org/
doi:10.1088/1367-2630/9/7/242

Abstract. We demonstrate sub-millijoule-energy, sub-4 fs-duration near-infrared laser pulses with a controlled waveform comprised of approximately 1.5 optical cycles within the full-width at half-maximum (FWHM) of their temporal intensity profile. We further demonstrate the utility of these pulses for producing high-order harmonic continua of unprecedented bandwidth at photon energies around 100 eV. Ultra-broadband coherent continua extending from 90 eV to more than 130 eV with smooth spectral intensity distributions that exhibit dramatic, never-before-observed sensitivity to the carrier-envelope offset (CEO) phase of the driver laser pulse were generated. These results suggest the feasibility of sub-100-attosecond XUV pulse generation for attosecond spectroscopy in the 100 eV range, and of a simple yet highly sensitive on-line CEO phase detector with sub-50-ms response time.

[3] Author to whom any correspondence should be addressed.

PII: S1367-2630(07)53044-2

Contents

Recently, attosecond metrology has been established as a viable means for time-resolving the fastest electronic processes known to occur in nature. The availability of isolated attosecond pulses is crucial to this approach [1]–[3]. Since the duration and intensity of these pulses fundamentally limits the temporal resolution that can be achieved in these experiments, efforts have been undertaken to further reduce the attosecond pulse duration to below 100 attoseconds and additionally, to improve the efficiency of their generation. Until now, isolated attosecond pulses have been produced in the extreme ultra-violet (XUV) region of the spectrum through the process of high-harmonic generation (HHG) in noble gasses. HHG can be described by the re-collision picture, in which the field of an intense near-infrared (NIR) laser pulse frees an electron by tunnel ionization, accelerates it in the continuum, and finally reunites it with its parent ion after the laser field changes its sign. Upon recombination, the excess energy gained by the electron from the NIR field, while in the continuum, is released as a burst of XUV radiation [4]. This series of steps is triggered during every half-cycle of the driving laser electric field, resulting in the emission of a train of XUV bursts spaced in time by the half-period of the laser field oscillation.

1. Isolated attosecond XUV pulse generation

To generate isolated XUV pulses by HHG, the emission pulse train must be truncated, either by using near single-cycle NIR driver laser pulses [2, 5] or by a technique known as polarization gating [6, 7], which relies on the sensitivity of HHG to the driver laser polarization. The latter technique has recently led to the generation of near transform-limited, 130 as, isolated attosecond XUV pulses [3]. Unfortunately, however, the photon energy and intensity of these pulses is relatively low, due to the inefficiency of the polarization-gating technique, which limits the applicability of these attosecond pulses. Another promising method for generating a suitable XUV continuum by HHG, from which even shorter isolated attosecond XUV pulses can be filtered, is by mixing the NIR driver pulse with a small amount of its second harmonic [8, 9]. This way, symmetry conditions within the fundamental optical pulse will be broken, and for even relatively long pulses high-energy XUV photons are emitted during only a single half-cycle of the optical pulse.

In this work, we build on previous efforts in generating isolated attosecond XUV pulses that utilized near single-cycle, ∼5 fs, waveform-controlled driver laser pulses [10]. We build on this work by employing even shorter driver pulses with durations below 4 fs and a carrier-wavelength

of approximately 0.7 μm. We expect that under these conditions, which more closely approach the single-cycle limit, isolated XUV pulses with durations comparable to that achieved with polarization gating, but with significantly higher photon energies and fluxes can be generated. Our conclusions are based on the observed ultra-broadband continuum in the XUV spectra generated by HHG using these new driver pulses.

In addition to the broadened XUV continuum, the use of shorter driver laser pulses will allow extension of the useable (i.e. sufficient flux) XUV radiation to higher photon energies. Although ionization is a prerequisite of HHG, it has long been recognized that an excess of free electrons in the interaction region is detrimental to the phase-matching of the HHG process. Additionally, generation of the highest energy harmonics requires that a significant fraction of the interaction atoms remain neutral until the peak intensity of the laser pulse is reached. By shortening the laser pulse, efficient ionization of the nonlinear media is constrained to the few half-cycles of the laser field that have the highest amplitude, reducing the overall ionization probability. Subsequently, more of the atoms will remain neutral in the strong NIR driving laser field until the moment when generation of the highest energy harmonics can occur.

2. Generation of waveform controlled sub-4 fs NIR driver pulses

Although the benefits of shorter driver pulses on isolated attosecond XUV pulse production have been expected, until now, suitable NIR pulses with durations significantly below 5 fs and enough energy for HHG have been unavailable to provide confirmation of these effects. At nanojoule energy levels, spectral bandwidth in the NIR region supporting few-cycle pulses can be generated in laser oscillators with proper dispersion management due to the broad gain bandwidth of Ti:sapphire [11]. Upon amplification to the millijoule (mJ) level (appropriate for HHG), however, this spectral bandwidth is lost due to gain-narrowing. Therefore, an additional step is necessary to generate a supercontinuum of visible and NIR frequency components, which can then be compressed, leading to near single-cycle ∼mJ pulses. The supercontinuum is generated by self-phase modulation (SPM), occurring in a noble-gas filled hollow-core fiber (HCF) [12] or in a self-guided filament [13]. Subsequent temporal compression can be performed using fixed-dispersion negative chirped mirrors or a more complicated but flexible adaptive compression scheme. To date, the shortest pulses ever generated have been at the ∼μJ level using adaptive pulse compression resulting in NIR pulse durations below 3 fs [14]. However, pulse energies of several μJ are not suitable for HHG and adaptive pulse compression is not easily implemented at ∼mJ pulse energies (∼200 microjoule). In comparison, at ∼mJ pulse energies, broadened spectra supporting pulses as short as ∼4 fs [15] were generated. However, this effort required two separate stages of spectral broadening by SPM and pulse re-compression, resulting in significant energy loss, or reduced efficiency. Furthermore, this multi-stage scheme is relatively complicated, inhibiting reliable control of the NIR waveform within the compressed pulse envelope. Therefore, these approaches are not ideally suited for use in attosecond spectroscopy experiments.

Spectral broadening in noble gasses is strongly dependent on the input pulse parameters. In general, shorter input pulses with larger initial bandwidth can be expected to be broadened more smoothly and more efficiently. Therefore, we sought to improve the output pulse characteristics of our commercial 3 kHz, ∼1 mJ chirped-pulse-amplification [16] laser system (Femtopower Compact Pro, Femtolasers GmbH). In its standard configuration the system uses a prism-based compressor following amplification of stretched Ti:sapphire oscillator seed pulses.

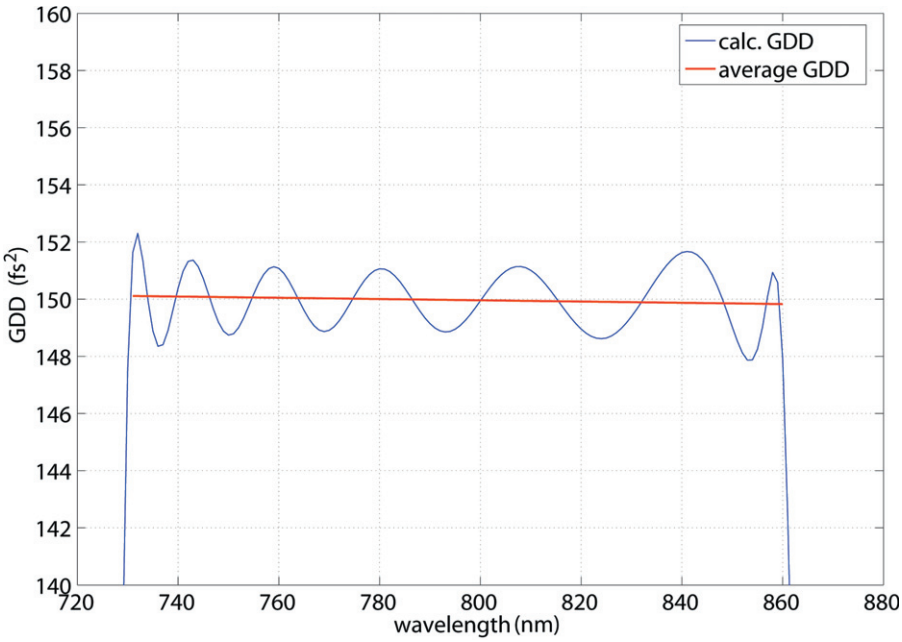

Figure 1. Design target for the positive dispersive mirrors used in the hybrid chirped mirror/prism compressor. Each reflection is designed to impart an average GDD of 150 fs^2. For comparison, 1 mm of fused-silica glass imparts ~40 fs^2 at 800 nm.

In the standard system, the amplified pulses enter the prism compressor positively chirped with a ~10 ps duration. The compressor introduces enough negative group-delay dispersion (GDD) such that the pulses enter the final prism with a slight negative chirp. At this point, upon propagation through the last prism, the bulk material introduces positive GDD to compensate the negative chirp and the pulses become maximally compressed. Because the pulses approach and reach their best compression inside the bulk material, SPM can occur even at modest pulse energies. In contrast to SPM in the HCF, in this case SPM manifests itself in the final prism as spectral narrowing due to the negative pre-chirp of the laser pulses [17].

To overcome the detrimental effects of SPM, we added a positive-dispersion chirped-mirror compressor to our standard Ti:sapphire amplifier system following the prism compressor. In this scheme, we modified the existing prism compressor to introduce even more negative group-delay dispersion allowing the laser pulses to maintain their negative chirp throughout the final prism. The pulses are then only fully compressed in the positive-dispersion mirror compressor where SPM does not occur. The mirrors are designed to impart 150 fs^2 of GDD per reflection from 730 nm to 860 nm, and higher order dispersion was minimized. The chirped mirror design target is shown in figure 1. A total of 14 reflections are used in the compressor, by which we estimate that the laser pulse exits the compressor stretched to at least 10 times the transform limit, to approximately 250 fs.

Using this hybrid compressor 930 μJ, sub-23 fs (full width at half maximum (FWHM)) pulses are delivered, where the duration was measured by second-order interferometric autocorrelation with an assumed Gaussian pulse shape. Spectral features indicative of SPM are absent and the output bandwidth is greater than 70 nm (FWHM), representing an improvement

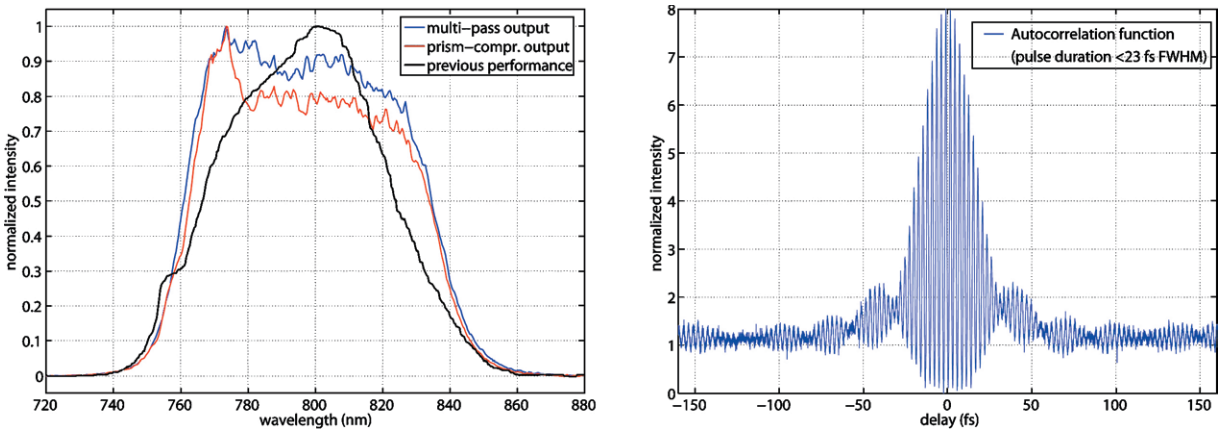

Figure 2. Femtopower output spectra. The black curve in the left panel is for comparison, showing typical performance achieved prior to implementation of the hybrid chirped-mirror/prism compressor. The notch in the spectrum near 760 nm and general spectral narrowing in comparison to the uncompressed amplified output indicate SPM. The blue and red curves show the current output spectrum achieved by using the hybrid chirped-mirror/prism compressor. The blue curve is the direct output from the multi-pass amplifier and the red curve is the spectrum following compression in the hybrid compressor. Gain narrowing due to SPM is minimized. In the right panel, the corresponding autocorrelation function measured using the hybrid compressor is shown. Compression to below 23 fs FWHM was reached. Uncompensated higher order dispersion is also evident, indicating that better compression can be achieved in the future.

of approximately 20 nm, or 40%, over the standard prism compressor system at these energies. Previously the bandwidth had been limited by spectral narrowing due to SPM. The output spectrum at the exit of the hybrid compressor and corresponding autocorrelation are shown in figure 2.

Following the hybrid prism compressor, the ∼1 mJ pulses are spectrally broadened in a 250-μm-inner-diameter HCF filled with 1.8 or 2.0 bar of Ne. Approximately 50% transmission is achieved. HCF output spectra for the two conditions used in our work, which are much broader, smoother and more blue-shifted than that obtained in previous efforts, are plotted in figure 3. These spectra, generated with 1.8 bar and 2.0 bar of Ne both support 3 fs (FWHM) transform-limited pulses, although the pulse envelope is not as ideal in the case of 1.8 bar due to the slightly narrower supercontinuum. The spectrally broadened pulses are compressed in a negative-GDD chirped-mirror compressor, which was designed for high reflectivity and well-controlled dispersion between 550 and 1000 nm. As a result, we cannot expect that the spectral components below 550 nm (the continuum extends to nearly 400 nm) will contribute to shortening of the compressed pulse. In spite of this slight limitation, remarkably good compression was achieved upon propagation in this chirped mirror compressor. Furthermore, new negative dispersion chirped mirrors have since been designed for the spectral range spanning 450 nm to 1000 nm and are now available for use, allowing the entire spectrum to contribute to the compressed pulse.

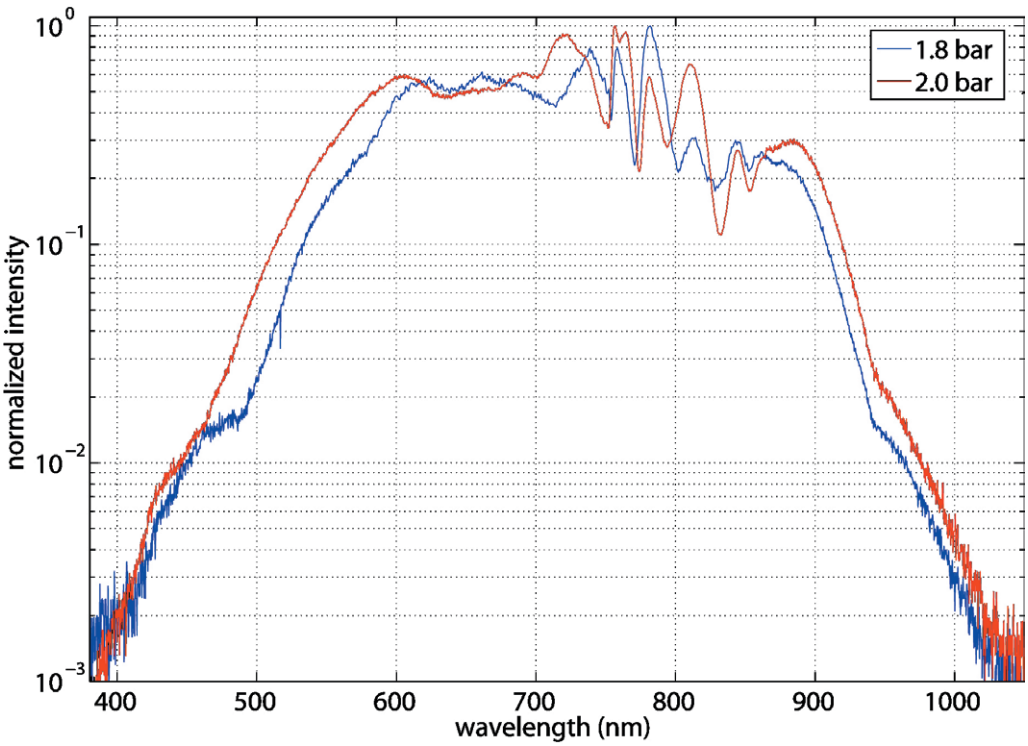

Figure 3. HCF broadened supercontinuum spectra utilizing shorter input pulses from the hybrid chirped-mirror/prism compressor. The blue curve shows the spectral broadening achieved using 1.8 bar of Ne while the red curve shows that achieved using 2.0 bar of Ne. The shortest SHG autocorrelation was measured using 2.0 bar Ne, while the shortest THG autocorrelation was achieved using 1.8 bar of Ne.

3. Characterization of sub-4 fs driver pulses

Measurements using a second-harmonic generation (SHG) interferometric autocorrelator as well as a third-harmonic generation (THG) interferometric autocorrelator were made to characterize the compressed supercontinuum. The nonlinear crystal in the SHG autocorrelator is a 20-μm-thick BBO crystal and suffers from phase-matching limitations for input pulses below 5 fs. Therefore, SHG autocorrelations were made primarily for use as a daily comparative diagnostic and for more general comparison with other published results, rather than for absolute pulse duration determination. The shortest SHG autocorrelations were obtained using the supercontinuum generated with 2.0 bar of Ne. A typical result is shown in figure 4. The transform-limited autocorrelation function was calculated based on the supercontinuum spectrum and is superimposed on the measured autocorrelation. It corresponds to a pulse duration of 3.0 fs FWHM. Remarkably, with a carrier wavelength of 720 nm, this pulse duration corresponds to a 1.25-cycle pulse.

Additional measurements were made using a THG autocorrelator. The THG autocorrelator can be used for characterization of pulses with durations below 5 fs because it utilizes a nonlinear surface effect. Surface THG on glass substrates [18]–[20] does not suffer from phase matching limitations because the reflected harmonic radiation originates from a sub-micrometer layer.

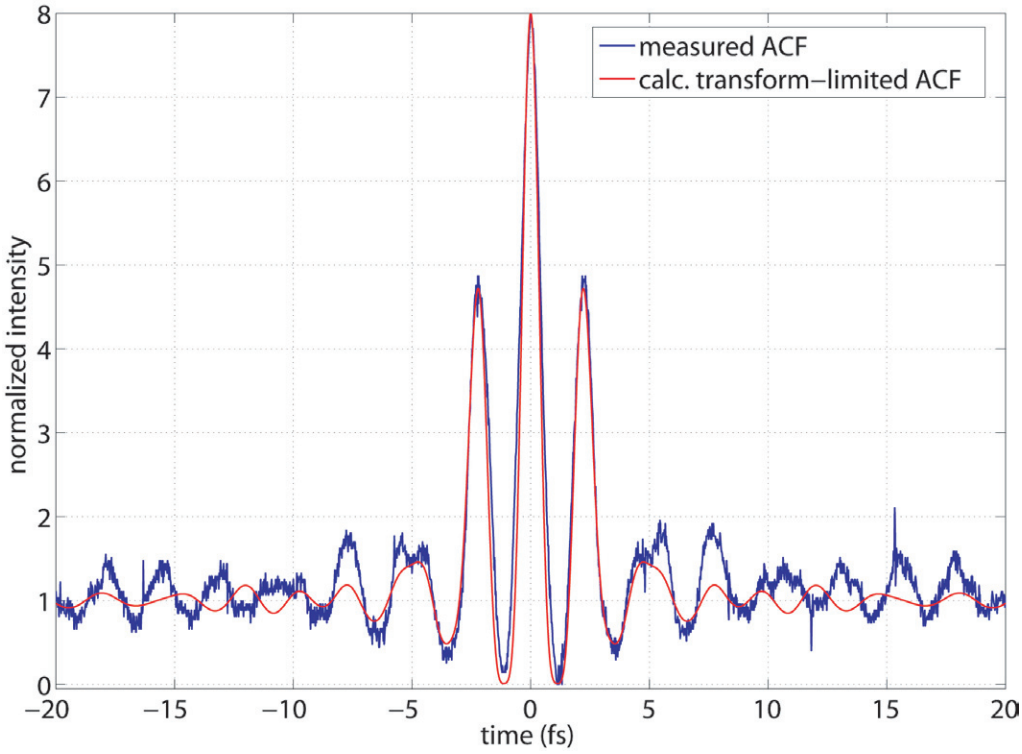

Figure 4. SHG interferometric autocorrelation of the compressed HCF output supercontinuum generated in 2.0 bar of Ne. The blue curve is the measured autocorrelation function. The red curve is the calculated transform limited autocorrelation function based on the input spectrum. The calculated pulse duration is 3.0 fs (FWHM), or with a carrier wavelength of ∼720 nm, 1.25 optical cycles.

Furthermore, the measured THG autocorrelation depends on the 6th power of the fundamental field. Therefore, the THG autocorrelation is more sensitive to the exact optical pulse shape than the SHG autocorrelation [21].

In the THG autocorrelator used in these measurements, two replicas of the input optical pulse are produced by a dispersion-minimized Michelson interferometer using ultra-broadband dielectric beamsplitters, and subsequently focused onto a quartz substrate coated with TiO_2 on the back surface. The 3rd harmonic of the incident radiation is generated in the TiO_2 layer and separated from the fundamental radiation using three dichroic mirrors. The transmitted 3rd harmonic signal is detected using a photomultiplier tube. The spectral acceptance of the THG autocorrelator is, however, limited in the short wavelength range below 570 nm in the input spectrum as the 3rd harmonic of this radiation is absorbed in air. For long input wavelengths, the THG autocorrelator is limited above 1000 nm by the sensitivity of the photomultiplier tube and reflectivity of the dichroic mirrors.

Using the THG autocorrelator, the shortest autocorrelation functions were obtained with the HCF supercontinuum generated at a Ne gas pressure of 1.8 bar. In this case, sub-4 fs (FWHM) pulses with 400 μJ pulse energy were measured. A typical measurement including a calculated THG autocorrelation function is shown in figure 5. The fitted curve was calculated assuming a Gaussian pulse shape and Fourier-limited pulse duration of 3.8 fs FWHM.

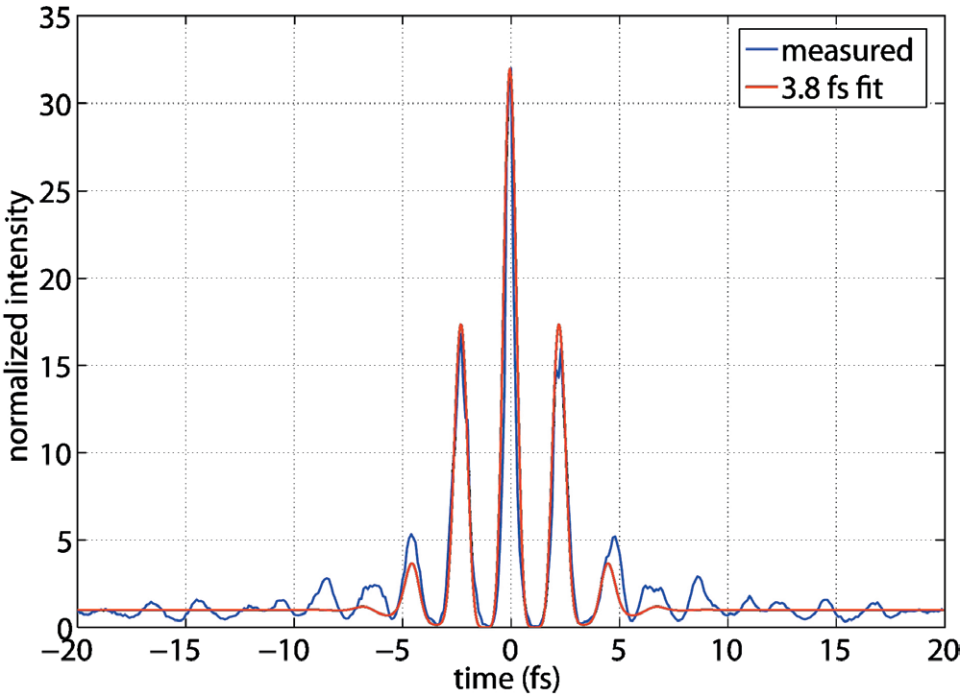

Figure 5. THG interferometric autocorrelation function of the compressed HCF output supercontinuum generated in 1.8 bar of Ne. The blue curve is the measured autocorrelation function. The red curve is the *fitted* transform limited autocorrelation function. The fit pulse duration is 3.8 fs (FWHM).

Although neither the SHG nor THG autocorrelators were completely free of limitations in characterizing these ultra-broadband pulses, both measurements set 4 fs as a reliable upper limit on the NIR driver pulse duration. Next, unique XUV spectra were produced by HHG providing confirmation that these driver pulses are significantly shorter than those used in previous experiments.

4. Generation and measurement of XUV spectra

Waveform-controlled sub-4 fs laser pulses generated using the hybrid compressor are focused with a silver mirror of a focal length of 40 cm through a thin fused silica window onto a jet of Ne gas inside a vacuum chamber as shown in figure 6. Neon is the interaction medium in which the HHG occurs. The delivered on-target energy is $\sim$300 μJ. The on-target intensity is dictated by the harmonic photon energy to be produced. The gas jet is formed by a metal tube, $\sim$2 mm inner diameter with two small holes ($\sim$150 μm) opposite to each other in radial direction, which is backfilled with Ne gas. The target can be moved along the optical axis to optimize the HHG process. The optimum working backpressure in the gas jet was found to be $\sim$350 mbar resulting in a significant flow of Ne into the vacuum chamber. With a vacuum pumping scheme designed for high gas loads, and working at these backpressures, the residual background pressure in the HHG chamber is maintained at 8×10^{-2} mbar, which is important to minimize reabsorption of the XUV radiation upon propagation to the experiment chamber.

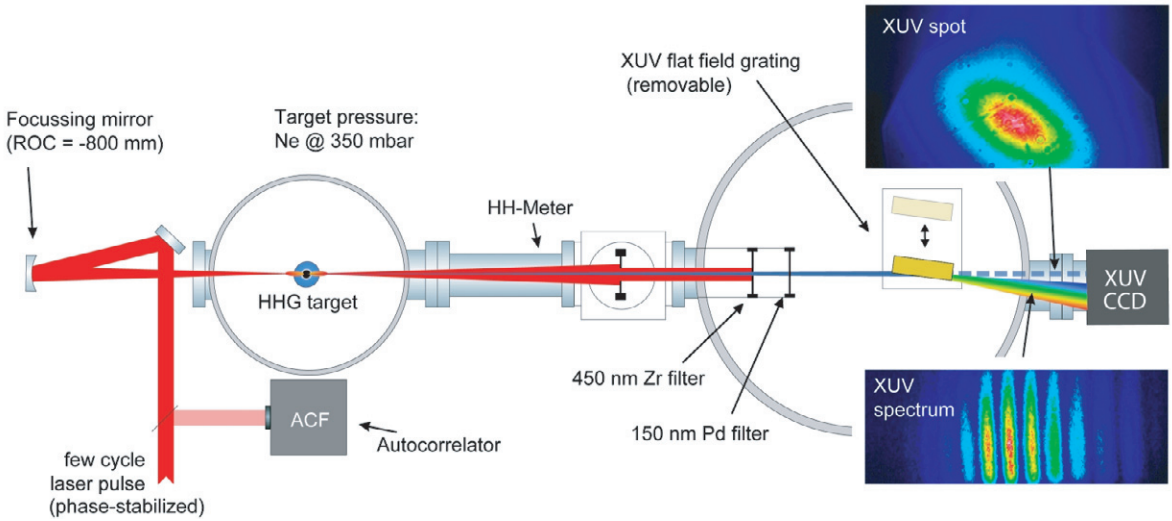

Figure 6. Few-cycle waveform-controlled NIR laser pulses are focused into a noble gas target (Ne) to produce high harmonic radiation. The pulse shape can be monitored using an interferometric autocorrelator. The 'HH-Meter' analyzes ionization of the background gas in the differential pumping stage and is indicative of the total XUV flux. After HHG, the remaining NIR radiation and low-order harmonics are filtered completely by a thin Zr and Pd foil. A back-thinned XUV camera (Roper Scientific) is used to observe either the direct XUV beam and/or by moving a flat-field grazing incidence grating (Hitachi) into the beam to observe the XUV spectrum.

Following HHG, the driver NIR laser pulse and the train of sub-fs XUV bursts co-propagate in a differential pumping stage, which is used to maintain a pressure gradient of six orders of magnitude between the HHG and experiment chambers. Upon entering the experiment chamber, the NIR laser light and low-order harmonics are filtered by use of a high-pass filter. The radiation is incident first on a 450 nm Zr foil, which is used to filter out the NIR driver pulse and isolate the cut-off region of the XUV spectrum. The Zr foil begins transmitting radiation at ~60 eV and has a relatively flat, near-peak transmission between ~90 eV and 160 eV, which extends beyond our expected cut-off region. Our apparatus also includes an additional 150 nm Palladium (Pd) foil, which was installed for use in a separate experiment investigating multilayer mirror coatings. The Pd filter begins transmitting radiation at ~90 eV, below the region of interest, and remains open until well beyond ~300 eV.

In the experiment chamber, the transmitted XUV radiation is wavelength-dispersed by a gold-coated XUV flat-field reflection grating mounted at grazing incidence. The intensity in the zero-order diffraction can be monitored as an overall measure of the XUV intensity using an X-ray CCD camera (Roper Scientific). To monitor the first-order diffracted XUV spectrum, the camera is rotated about a pivot point underneath the XUV grating to the appropriate region of the spectrum. To acquire the XUV spectra shown in figure 7, the CCD integration time was set to 50 ms, allowing the accumulation of 150 shots per spectrum and the camera pixels were binned vertically for fast readout.

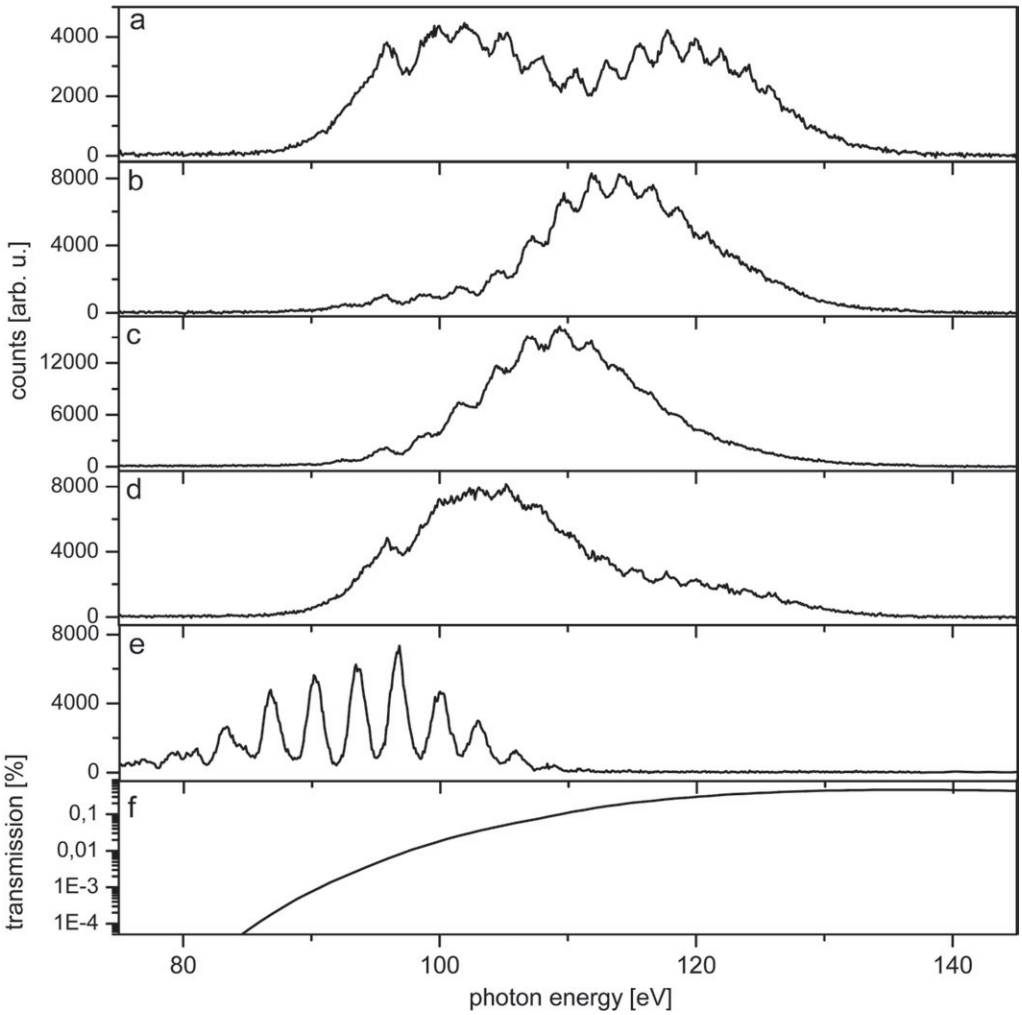

Figure 7. CEO phase dependence of the XUV spectrum. A XUV spectrum for an initial value φ_0 of CEO phase, which we believe is close to zero (corresponding to a near cosine-shaped waveform), is shown in panel (a). Corresponding spectra for the CEO phases $\varphi = \varphi_0 + \pi/4$, $\varphi = \varphi_0 + \pi/2$ and $\varphi = \varphi_0 + 3\pi/4$, are shown in panels (b), (c), and (d), respectively. In general, the spectral features are strongly dependent on the CEO phase and the effective cut-off energy shifts by more than 10 eV as the CEO phase is varied. An XUV spectrum generated by relatively long NIR driver pulses is shown in panel (e). Deep modulation in this HHG spectrum, which coincides with the use of long driver pulses, demonstrates the resolution of our spectrometer. Panel (f) shows the transmission function of the 150 nm thick Pd filter over the relevant spectral range (the transmission of the Zr foil is nearly flat in this spectral region).

5. Ultra-broadband highly phase-sensitive XUV spectra

To investigate the dependence of the resultant XUV spectrum on the carrier-envelope offset (CEO) phase of the driver NIR laser pulse, XUV spectra were recorded for different settings of the CEO phase. Figure 7 shows characteristic XUV spectra recorded at four different settings

of the CEO phase, from $\varphi = \varphi_0 \approx 0$ to $\varphi = \varphi_0 + 3\pi/4$, stepped in increments of $\pi/4$. Dramatic CEO phase dependence in the cut-off region is observed for our ultrashort ~1.5-cycle driver laser pulses. Variation in the CEO phase of the laser system strongly influences the shape of the spectrum and results in a shift of the XUV cut-off energy by more than 10 eV. Figure 7(a) shows the CEO phase and corresponding spectrum for which the highest cut-off energy was achieved. This CEO phase was defined as $\varphi = 0$. In this spectrum, two dominant peaks separated by ~20 eV are clearly evident. As the CEO phase is slowly varied between zero and π, this double-humped structure vanishes as the higher energy peak becomes enhanced (shown in panel (b)), next the middle portion of the spectrum that had previously been minimized at $\varphi = 0$ becomes enhanced (shown in panel (c)), and finally the low energy peak becomes prominent (shown in panel (d)), followed by a revival of the original double-humped spectrum. This behaviour is periodic and observed to repeat upon subsequent full π-phase shifts.

Notably, for all settings of the CEO phase, the high-energy XUV continuum is maintained with only a small amplitude modulation in the most extreme case. This behaviour is not a result of poor instrument resolution as evidenced by the spectrum shown in figure 7(e). Here, a deeply modulated XUV spectrum is shown for reference and was generated by a relatively long driver laser pulse (~10 fs) resulting from reduced Ne gas pressure in the HCF. Using ultrashort sub-4 fs driver pulses, the XUV continuum in the cut-off region has been substantially broadened, extending from ~90 eV to over 130 eV. By suitable XUV filtering of the ultra-broad bandwidth generated by these unique driver pulses, and by proper compression of the spectral phase, these advances in HHG will permit the generation of sub-100 as XUV pulses at photon energies well above 100 eV.

We attribute the observed sensitivity in the XUV cut-off region to the shift of the individual half-cycle cut-offs [22] within the driving laser pulse. A half-cycle cut-off refers to the highest XUV photon energy that can be reached upon an electron re-collision within a particular half-cycle of the laser field. The variation between adjacent half-cycle cut-offs is more pronounced for shorter laser pulses. The key parameter is the steepness of the pulse envelope compared with the oscillation cycle. This quantity determines the variation of the electric field amplitude from one half-cycle to the next. For our ~1.5-cycle driver pulses, the main and the adjacent half-cycle cut-off energy may differ by as much as 27 eV according to a classical trajectory analysis.

Beyond the extended cut-off region generated by these 1.5-cycle driver laser pulses, the observed sensitivity of the features in the XUV spectrum may serve as a useful on-line monitor of the CEO phase of the driver laser pulse in attosecond spectroscopic systems. Moreover, because the spectral features are so pronounced, it is currently possible to easily determine the CEO phase dependence of the spectrum after an acquisition time of only 50 ms, which is the fastest integration time possible using the current XUV CCD camera. Based on the observed photon count rates, with a faster detector, it would be possible to observe the relevant features in a fraction of the current detector-limited 50 ms integration time. In the absence of detector limits, the integration time could be further reduced by using thinner Zr high-pass filters, which we use to isolate the XUV radiation from the driving NIR pulse, because thinner Zr foils are equally effective in filtering the NIR from the XUV radiation, but would transmit more of the XUV radiation. If all of these steps are implemented, it is conceivable that the extreme sensitivity of the XUV spectrum could be utilized to make CEO phase measurements within only tens of XUV bursts.

6. Conclusions and outlook

We have reported on a novel hybrid prism/chirped-mirror compressor, which represents a significant step forward towards the generation of intense near single-cycle NIR laser pulses from a simple and reliable laser system. Furthermore, our preliminary HHG experiments reveal a never-before-observed dramatic dependence of the coherent soft-X-ray emission on the precise shape of the underlying laser waveform. These results demonstrate the potential of intense near-single-cycle laser fields for the generation of isolated sub-100-as XUV pulses powerful enough for attosecond spectroscopy.

Acknowledgments

This work was supported by the Deutsche Forschungsgemeinschaft (DFG) in the frame of the excellence cluster 'Munich Centre for Advanced Photonics' (MAP www.munich-photonics.de), by the European Commission Integrated Infrastructure Initiative LASERLAB-Europe, and the Marie Curie Research Training Network XTRA (MRTN-CT-2003 505138). EG acknowledges an Intra-European Marie-Curie fellowship MEIF-CT-2005-024440. The authors acknowledge support concerning the CEP stabilization from MENLO Systems GmbH.

References

[1] Hentschel M, Kienberger R, Spielmann Ch, Reider G A, Milosevic N, Brabec T, Corkum P, Heinzmann U, Drescher M and Krausz F 2001 *Nature* **414** 509
[2] Kienberger R *et al* 2004 *Nature* **427** 817
[3] Sansone G *et al* 2006 *Science* **314** 443
[4] Corkum P B 1993 *Phys. Rev. Lett.* **71** 1994
[5] Christov I P, Murnane M M and Kapteyn H C 1997 *Phys. Rev. Lett.* **78** 1251
[6] Shan B, Ghimire S and Chang Z 2005 *J. Mod. Opt.* **52** 277
[7] Sola I J *et al* 2006 *Nature Physics* **2** 319
[8] Oishi Y, Kaku M, Suda A, Kannari F and Midorikawa K 2006 *Optics Express* **14** 7230
[9] Pfeifer T, Gallmann L, Abel M J, Nagel P M, Neumark D M and Leone S R 2006 *Phys. Rev. Lett.* **97** 163901
[10] Baltuška A *et al* 2003 *Nature* **421** 611
[11] Fuji T, Unterhuber A, Yakovlev V S, Tempea G, Krausz F and Drexler W 2003 *Appl. Phys.* B **77** 125
[12] Nisoli M, De Silvestri S and Svelto O 1996 *Appl. Phys. Lett.* **68** 2793
[13] Hauri C P, Kornelis W, Helbing F W, Heinrich A, Couairon A, Mysyrowicz A, Biegert J and Keller U 2004 *Appl. Phys.* B **79** 673
[14] Yamashita M, Yamane K and Morita R 2006 *IEEE Journ. Sel. Topics in Quant. Electron.* **12** 213
[15] Cheng Z, Tempea G, Brabec T, Ferencz K, Spielmann Ch and Krausz F 1999 *Ultrafast Phenomena XI* ed T Elsässer, J G Fujimoto, D A Wiersma and W Zinth (Berlin: Springer) p. 8
[16] Strickland D and Mourou G 1985 *Opt. Commun.* **56** 219
[17] Planas S A, Pires Mansur N L, Brito-Cruz Carlos H and Fragnito H L 1993 *Opt. Lett.* **18** 699
[18] Tsang T Y F 1995 *Phys. Rev. A: At. Mol. Opt. Phys.* **52** 4116
[19] Stoker D, Becker M F and Keto J W 2005 *Phys. Rev. A: At. Mol. Opt. Phys.* **71** 061802R
[20] Squier J A, Fittinghoff D N, Barty C P J, Wilson K R, Muller M and Brakenhoff G J 1998 *Opt. Comm.* **147** 153
[21] Meshulach D, Barad Y and Silberberg Y 1997 *J. Opt. Soc. Am. B: Opt. Phys.* **14** 2122
[22] Haworth C A, Chipperfield L E, Robinson J S, Knight P L, Marangos J P and Tisch J W G 2007 *Nature Physics* **3** 52